# Determination of the Interaction Potential and Rovibrational Structure of the Ground Electronic State of MgAr+ Using PFI-ZEKE Photoelectron Spectroscopy

Dominik Wehrli, Matthieu Génévriez, Carla Kreis, Josef A. Agner, and Frédéric Merkt*

Laboratory of Physical Chemistry, ETH Zürich, CH-8093 Zürich, Switzerland

S *Supporting Information*

ABSTRACT: The interaction potential characterizing the ground electronic state of MgAr+ has been determined from the photoelectron spectrum recorded from the a $^3\Pi_0$ metastable state of MgAr at high resolution by pulsed-field-ionization zero-kinetic-energy (PFI-ZEKE) photoelectron spectroscopy. The photoelectron spectrum provides information on the first ten vibrational levels of MgAr+ and leads to the determination of the adiabatic ionization energy of metastable MgAr (38 742.3(20) cm^{-1}), the ground state dissociation energy of MgAr+ (1254(60) cm^{-1}), and to the characterization of the rovibrational photoionization dynamics of MgAr.

Mg+(3s)·Ar X+ $^2\Sigma^+$
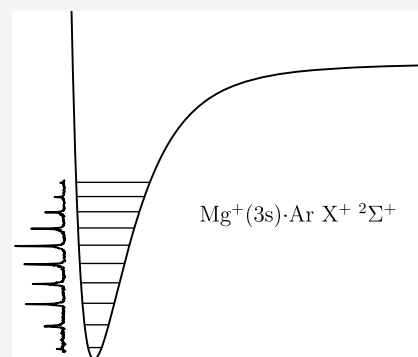
1. INTRODUCTION

Molecular complexes involving rare gases and positively charged alkali and alkaline-earth metal atoms serve as model systems to study fundamental aspects of chemical binding mechanisms, solvation, metal−ligand interactions, and the interactions of atoms at metal surfaces.[1,2] Considerable effort has therefore been invested in the past 25 years to characterize molecules of the type M+·Rg (M+ = Be+, Mg+, Ca+, etc. and Rg = He, Ne, Ar, Kr, etc.) in spectroscopic and mass-spectrometric experiments and through ab initio quantum-chemical calculations (see refs 1, 2 and references therein). Initial interest in the properties of MgAr+ can be traced to the first observation of the photoionization spectrum of MgAr by Massick and Breckenridge[3] and of the electronic spectrum of MgAr+ by Duncan and co-workers.[4−7] Both MgAr and MgAr+ are easily formed and entrained in supersonic beams following laser ablation of Mg atoms in the presence of Ar gas,[4,8] which greatly facilitates investigations of their properties by spectroscopy and mass spectrometry.

Despite these studies, the experimental data available on MgAr+ appear to be limited to high-resolution recordings of the Mg+(3p)·Ar A+ $^2\Pi_{1/2,3/2}$ ← Mg+(3s)·Ar X+ $^2\Sigma^+$ (v^+ = 0) band system[4−7] and to the determination of the adiabatic ionization energy of the Mg(3s3p)·Ar a $^3\Pi_0$ metastable state.[3] The only experimental information on the electronic ground state of MgAr+ thus consists of (i) the rotational structure of the ground vibrational level and the first vibrational interval determined from the A+ ← X+ band system,[6,7] (ii) its position relative to the Mg(3s3p)·Ar a $^3\Pi_0$ metastable state determined from the onset of MgAr+ in the photoionization spectrum,[3] and (iii) its dissociation energy, obtained from the dissociation energy of the Mg+(3p)·Ar A+ $^2\Pi_{1/2,3/2}$ state using a thermochemical cycle[4−6,9]

and from measurements of the velocity distribution of the Mg+ fragments produced by photolysis of MgAr+.[10] Information on the energy-level structure of MgAr+ has also been obtained in theoretical studies.[2,9,11,12]

We report on an experimental study of the Mg+(3s)·Ar X+ $^2\Sigma^+$ state by high-resolution pulsed-field-ionization zero-kinetic-energy (PFI-ZEKE) photoelectron spectroscopy, which has led to the observation of the v^+ = 0−9 vibrational levels and to the determination of an improved value of the adiabatic ionization energy of MgAr. The new data have been used to derive an empirical interaction potential for the ground state of MgAr+ and to determine its dissociation energy. In addition, the intensity distribution of the photoelectron spectrum provided information on the photoionization dynamics of the Mg(3s3p)·Ar a $^3\Pi_0$ metastable state.

2. EXPERIMENTAL SETUP

The experimental setup has been described in detail in ref 13 and includes a laser-ablation source of Mg atoms, a Nd:YAG-pumped dye laser, and a detection system for the photoelectrons and photoions produced following photoexcitation. Metastable MgAr molecules in the Mg(3s3p)·Ar a $^3\Pi_0$ state were generated by laser ablation with a frequency-doubled Nd:YAG laser (pulse energy ∼2 mJ) of a magnesium rod in a supersonic beam of Ar (nozzle-stagnation pressure ∼1 bar) using a high-intensity pulsed molecular-beam valve.[14] MgAr was formed in situ among larger MgAr$_n$ clusters (n > 1). The formation of metastable

MgAr in a similar laser-ablation source was first described by Bennet et al.,[8,15] who also observed the singlet $Mg(3s^2)\cdot Ar\ X\ ^1\Sigma^+$ ground state. The molecules passed through a 3 mm diameter skimmer located 8 cm downstream from the ablation spot and entered the photoexcitation chamber. In this chamber, the supersonic beam intersected the laser beam used for photoexcitation at right angles within a cylindrical electrode stack used to apply pulsed electric fields. These pulses served the purpose of field-ionizing high Rydberg states and extracting photoelectrons or photoions into a time-of-flight spectrometer at the end of which they were detected with a microchannel-plate assembly.

We tripled the frequency of the output of a Nd:YAG-pumped tunable dye laser using two BBO crystals and photoexcited metastable MgAr in the vicinity of the ionization thresholds corresponding to $Mg^+(3s)\cdot Ar\ X^+\ ^2\Sigma^+$ rovibrational levels, as depicted in Figure 1. The bandwidth of the laser was ~0.15

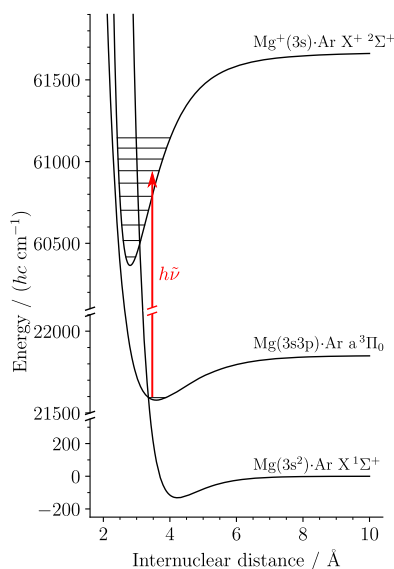**Figure 1.** Excitation scheme from the metastable $Mg(3s3p)\cdot Ar\ a\ ^3\Pi_0$ state to the $Mg^+(3s)\cdot Ar\ X^+\ ^2\Sigma^+$ state. The ionic potential curve was derived from the data measured in this work and ref 6, as explained in detail in Section 4.1. The potential curves corresponding to the neutral triplet and singlet states are Morse-type potentials based on the molecular parameters from ref 12.

cm^{-1}, the beam diameter at the photoexcitation spot was ~1 mm, and the pulse energy was ~0.5 mJ. The fundamental wavelength of the dye laser was calibrated using a commercial wavemeter with a specified accuracy of 0.02 cm^{-1}.

The method of PFI-ZEKE photoelectron spectroscopy[16,17] was used to measure spectra of the $Mg^+(3s)\cdot Ar\ X^+\ ^2\Sigma^+ \leftarrow Mg(3s3p)\cdot Ar\ a\ ^3\Pi_0$ ionizing transition. To record an overview spectrum of this transition, we used a two-pulse field-ionization sequence consisting of a discrimination pulse of +0.86 V/cm and a single field-ionization and extraction pulse of −1.38 V/cm, yielding a resolution of ~1.2 cm^{-1} (full width at half-maximum of the $Mg^+\ 3s\ ^2S_{1/2} \leftarrow Mg\ 3s3p\ ^3P_J$ ionizing transition, see below). A typical pulse sequence used to record high-resolution spectra of single vibrational bands consisted of a +0.52 V/cm discrimination pulse followed by pulses of −0.43, −0.46, −0.48, −0.51, −0.53, −0.56, −0.59, −0.61, −0.64, and −0.66 V/cm. Each extraction pulse gave rise to a distinct PFI-ZEKE photoelectron spectrum so that each laser scan led to the simultaneous recording of several spectra. The relatively strong

discrimination pulse was necessary to cleanly eliminate low-energy photoelectrons produced by autoionization and direct photoionization (called prompt electrons). To correct for the electric-field-induced shifts of the ionization thresholds, we recorded photoelectron spectra of the $Mg^+\ 3s\ ^2S_{1/2} \leftarrow Mg\ 3s3p\ ^3P_J$ transition under identical experimental conditions and extracted the shifts associated with the different pulses of the field-ionization sequence by comparing the experimental line positions with the well-known ionization energy of Mg.[18] After the field correction, the spectra obtained from the different pulses were added to increase the signal-to-noise ratio, without significantly degrading the spectral resolution of ~0.4 cm^{-1}. To further improve the signal-to-noise ratio, we repeated the recording of the high-resolution spectra several times under identical conditions and added them.

To unambiguously measure the isotopic shifts of vibrational levels, we employed the technique of mass-analyzed threshold-ionization (MATI) spectroscopy[19] and recorded spectra of $^{24}MgAr$, $^{25}MgAr$, and $^{26}MgAr$ after separation of the corresponding prompt ions in the time-of-flight spectrum. The two-pulse sequence used in this scheme consisted of a +1.72 V/cm discrimination pulse and a +69 V/cm extraction pulse. The isotopic shifts were then determined after fitting exponential functions

$$I_i(\tilde{\nu}) = \exp(-(\tilde{\nu} - \tilde{\nu}_{0,i})) \tag{1}$$

to the high-energy edges of the lines in the MATI spectra of ^iMgAr ($i = 24, 25, 26$) and taking differences of the fitted values of $\tilde{\nu}_{0,i}$. Each MATI spectrum was normalized to give equal maximum intensity, such that the differences corresponded exactly to the isotopic shifts. An example of such a fit is shown in the inset of Figure 2 as a red dashed line.

3. EXPERIMENTAL RESULTS

The photoionization spectrum of MgAr in the vicinity of the $Mg^+(3s)\cdot Ar\ X^+\ ^2\Sigma^+ \leftarrow Mg(3s3p)\cdot Ar\ a\ ^3\Pi_0$ ionization thresholds is shown in Figure 2a. In the figure, we distinguish between three regions, separated by dashed vertical lines. In region (i), only discrete autoionization resonances are visible over a zero background ionization signal from direct ionization. In region (ii), the direct-ionization signal gradually rises and so does the density of autoionization resonances. In region (iii), the photoionization signal remains approximately constant. We will discuss the implications of these general characteristic features in Section 4.2.

An overview PFI-ZEKE photoelectron spectrum of the $Mg^+(3s)\cdot Ar\ X^+\ ^2\Sigma^+ \leftarrow Mg(3s3p)\cdot Ar\ a\ ^3\Pi_0$ transition is presented in Figure 2b. The ionization energies $E_I(v^+)$ corresponding to the successive vibrational levels of the X^+ state are listed in Table 1 together with the vibrational term values $T_{v^+} = [E_I(v^+) - E_I(v^+ = 0)]/(hc)$. The vibrational assignment was made on the basis of the analysis of isotopic shifts presented below. For the adiabatic ionization energy of the $Mg(3s3p)\cdot Ar\ a\ ^3\Pi_0$ state, we found $E_I(v^+ = 0)/(hc) = 38\ 742.3(20)$ cm^{-1}, which is in agreement with the value of $38\ 744(5)$ cm^{-1} reported by Massick and Breckenridge.[3] The specified error of 2.0 cm^{-1} includes both statistical and systematic (wave number calibration, correction of the field-induced shifts, and perturbations of the rotational structure) uncertainties. The uncertainty in the T_{v^+} values is less than that of the ionization thresholds because systematic errors partially cancel out when building the differences between absolute ionization energies. From the term values T_{v^+}, we
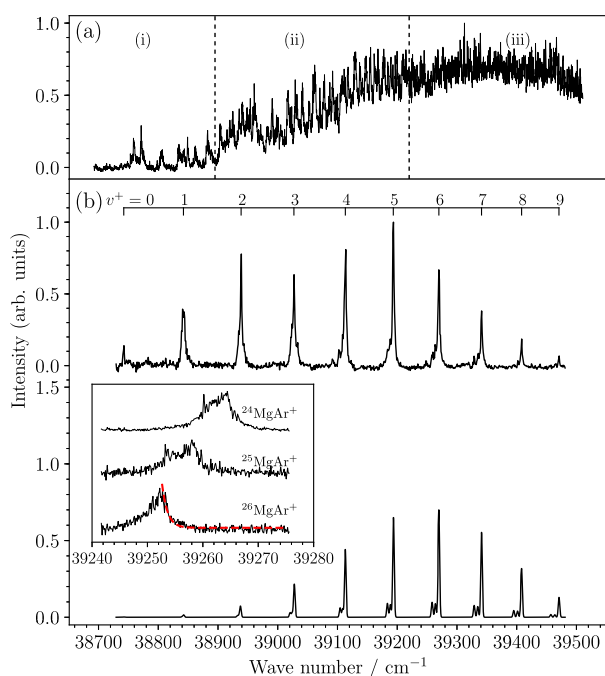
Figure 2. (a) Photoionization spectrum of MgAr in the vicinity of the $Mg^+(3s)\cdot Ar\ X^+\ ^2\Sigma^+ \leftarrow Mg(3s3p)\cdot Ar\ a\ ^3\Pi_0$ ionization threshold with the three distinct regions (i)−(iii) described in the text. (b) Measured (upper trace) and calculated (lower trace) overview PFI-ZEKE photoelectron spectra of the $Mg^+(3s)\cdot Ar\ X^+\ ^2\Sigma^+ \leftarrow Mg(3s3p)\cdot Ar\ a\ ^3\Pi_0$ ionizing transition. The calculations of Franck−Condon factors were performed using the potential curves shown in Figure 1. The measured intensities of transitions to low-v^+ states are much higher than predicted by the calculation because of channel interactions. The inset shows a MATI spectrum of the transition to the $v^+ = 6$ level of $^{24}MgAr^+$, $^{25}MgAr^+$, and $^{26}MgAr^+$, from which isotopic shifts and the absolute vibrational assignment were determined.

determined the vibrational constants $\omega_e = 104.49(17)$ cm^{-1} and $\omega_e x_e = 2.36(2)$ cm^{-1} of the $X^+\ ^2\Sigma^+$ state of $^{24}Mg^{40}Ar^+$ in a least-

squares-fit procedure. These values agree well with the theoretical values reported by Gardner et al.[21] ($\omega_e = 104.8$ cm^{-1} and $\omega_e x_e = 2.53$ cm^{-1}).

High-resolution PFI-ZEKE photoelectron spectra of the $v^+ = 3$ and 7 bands are depicted in Figure 3. The spectrum of the $v^+ = 3$ band reveals strong perturbations of the rotational structure caused by channel interactions, which we also observed for other bands with $v^+ < 5$ (regions (i) and (ii) in Figure 2a). These perturbations will be discussed in Section 4.2. The spectra of the $v^+ = 6$ (not shown) and $v^+ = 7$ bands did not exhibit such perturbations and were used to extract more accurate absolute ionization energies than those available from the overview spectrum. In Table 1, we list the average ionization energies for $v^+ = 6$ and 7 obtained from the analysis of high-resolution spectra. The transitions to the $v^+ = 0$, 8, and 9 levels of the ion were not intense enough to be measured in a multipulse experiment.

To obtain absolute assignments of the vibrational levels, we determined the isotopic shifts for the $v^+ = 6$ and 7 levels experimentally, as shown in Figure 4. The isotopic shifts were determined from both MATI and PFI-ZEKE photoelectron spectra. A MATI spectrum of the $v^+ = 6$ band is shown as an inset in Figure 2b. The shifts determined from the MATI spectra are shown as triangles in Figure 4. These shifts were then used to unambiguously assign the absolute values of the vibrational quantum number v^+. The isotopic shifts were also extracted from the PFI-ZEKE photoelectron spectra (not shown) and are indicated as circles in Figure 4.

4. DISCUSSION

4.1. Potential-Energy Function of the X$^+$ State. From the rovibrational structure of the photoelectron spectrum, we determined the potential-energy function of the $Mg^+(3s)\cdot Ar\ X^+\ ^2\Sigma^+$ state in a least-squares fit. We used an analytical function of the form

$$V(r) = A[e^{2B(1-r/C)} - 2e^{B(1-r/C)}] - \frac{\alpha_{Ar}}{2r^4}\Phi(r) \tag{2}$$

Table 1. Observed Ionization Energies $E_I(v^+)$ Corresponding to the $Mg^+(3s)\cdot Ar\ X^+\ ^2\Sigma^+\ (v^+) \leftarrow Mg(3s3p)\cdot Ar\ a\ ^3\Pi_0\ (v'' = 0)$ Ionizing Transitions of $^{24}MgAr$, $^{25}MgAr$, and $^{26}MgAr$, Term Values T_{v^+} of the Vibrational Levels of $^{24}MgAr^+$, and Comparison with Calculated Values ($\Delta T_{v^+} = T_{v^+}^{calc} - T_{v^+}^{exp}$) Obtained from the Analytical Potentials Given in eq 2[a,b]

v^+	$E_I(v^+)/(hc)^c$	$T_{v^+}^{exp\,c}$	$\Delta T_{v^+}^d$	$\Delta T_{v^+}^e$	$B_{v^+}^d$	$B_{v^+}^e$
0	38 742.3(20)	0.0	0.0	0.0	0.1409	0.139
1	38 842.2(20)	99.9(15)[f]	0.3	−0.4	0.137	0.135
2	38 938.7(20)	196.4(15)	−1.1	−2.3	0.132	0.131
3	39 027.1(20)	284.8(15)	0.7	−1.0	0.128	0.127
4	39 113.2(10)	370.9(6)	−0.1	−2.0	0.124	0.123
5	39 193.4(10)	451.2(6)	0.2	−1.8	0.120	0.119
6	39 269.0(4)[g]	527.5(6)	−0.1	−2.2	0.116	0.115
	39 262.9(4)[g] ($^{25}MgAr^+$)					
	39 257.7(4)[g] ($^{26}MgAr^+$)					
7	39 341.1(5)[g]	598.9(6)	0.0	−2.2	0.112	0.111
	39 334.7(5)[g] ($^{25}MgAr^+$)					
	39 328.8(5)[g] ($^{26}MgAr^+$)					
8	39 408.2(10)	665.9(6)	0.0	−2.2	0.108	0.107
9	39 470.7(10)	728.5(6)	0.1	−2.2	0.103	0.103

[a]In addition, the rotational constants B_{v^+} calculated from this potential are listed in the last two columns. [b]All values are in cm^{-1}. [c]Determined from the overview PFI-ZEKE photoelectron spectrum depicted in Figure 2b unless stated otherwise. [d]Using the potential parameters listed in Table 3 derived from the experimental data in a least-squares fit. [e]Calculated with the potential obtained by fitting eq 2 to the ab initio potential-energy values of Gardner et al.[21] (see the text for details). [f]Pilgrim et al. obtained a value of 96 cm^{-1} for T_1.[5] [g]Determined from the high-resolution PFI-ZEKE photoelectron spectra.
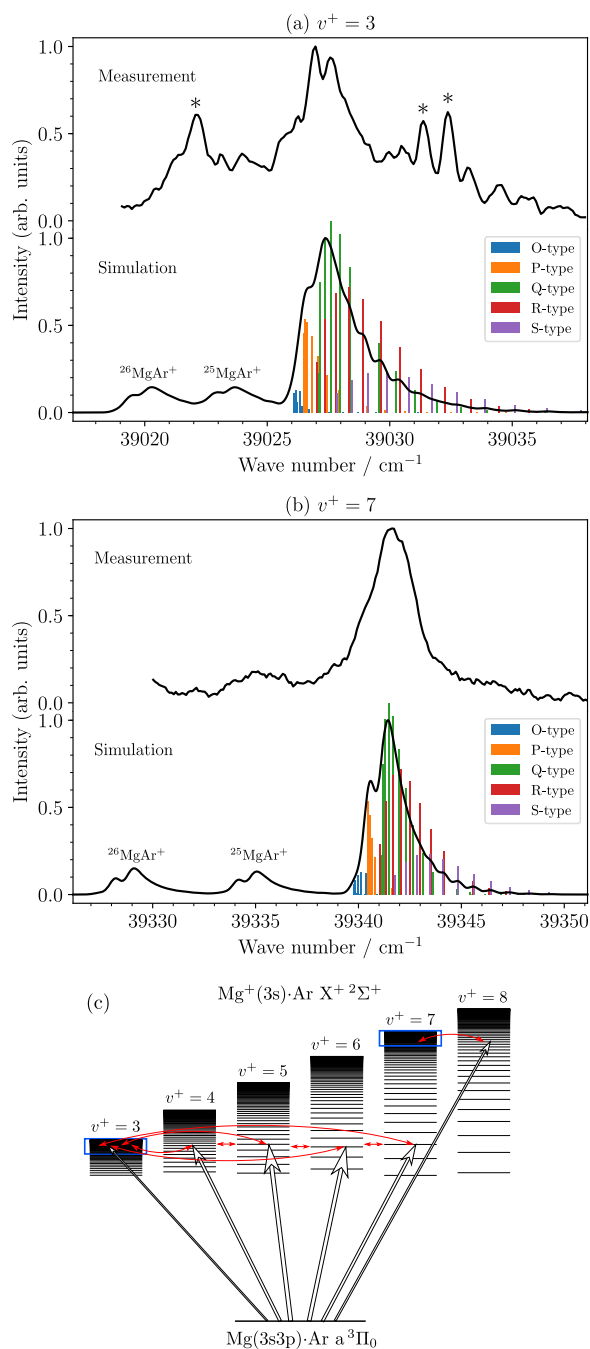
(a) $v^+ = 3$

(b) $v^+ = 7$

(c)

Figure 3. (a, b) High-resolution experimental (upper trace) and calculated (lower trace) PFI-ZEKE photoelectron spectra of the transitions to the $Mg^+(3s)\cdot Ar\ X^+\ {}^2\Sigma^+$, $v^+ = 3$ and 7 states. The calculation of the rotational structure was performed using the model of Buckingham et al.,[20] assuming photoionization from a pure p orbital, a rotational temperature of 3 K, and a resolution (full width at half maximum, FWHM) of 0.6 cm^{-1}. Whereas the calculated spectrum of the $v^+ = 7$ band is in agreement with the experimental spectrum and exhibits the isotope structure, the spectrum of the $v^+ = 3$ band reveals several perturbations (marked with asterisks) originating from the channel interactions illustrated in (c) (see the text for details).

where r is the internuclear distance. The first term in eq 2 corresponds to a Morse potential with dissociation energy A and equilibrium distance C, and the second term describes the charge-induced dipole interaction of Mg^+ and Ar, ensuring correct long-range behavior. The switch function
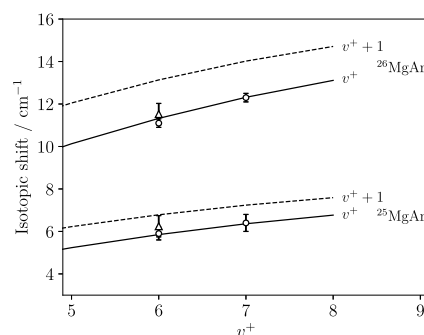

Figure 4. Isotopic shifts of the $v^+ = 6$ and 7 levels of ${}^{25,26}MgAr^+$ with respect to ${}^{24}MgAr^+$ determined from PFI-ZEKE photoelectron (circles) and MATI (triangles) spectra, respectively. The solid line is the prediction for the case that the lowest observed level corresponds to $v^+ = 0$ (see Figure 2b). The dashed line corresponds to the case where the lowest observed level would be $v^+ = 1$. The shifts were predicted from potential curves, which were fitted to the experimental data, as explained in Section 4.1.

$$\Phi(r) = \frac{1}{2}\left[1 + \tanh\left(\frac{r - D}{E}\right)\right] \tag{3}$$

turns off the charge-induced dipole interaction at short internuclear distances. The polarizability volume $\alpha_{Ar} = 11.08\ a_0^3$ of argon is well-known experimentally[22] and was not adjusted in the fit. The ab initio potential-energy curve provided as the supplementary material by Gardner et al.[21] served as a starting point to obtain initial values of the parameters A, B, C, D, and E in a least-squares fit. In this fit, we excluded the first four data points at short distances in the potential reported by Gardner et al. because the Morse-type function in eq 2 does not adequately model the repulsive part of the potential. This neglect has no significant effect on the bound states of the potential. The vibrational level energies (with rotational angular momentum $N = 0$) were determined by solving the Schrödinger equation describing the nuclear motion (in atomic units)

$$\left[-\frac{1}{2\mu}\frac{d^2}{dr^2} + V(r)\right]\psi_{v^+}(r) = E_{v^+}\psi_{v^+}(r) \tag{4}$$

using a Legendre−Gauss−Lobatto discrete-variable-representation (DVR) technique.[23−25] In eq 4, μ is the reduced mass of $MgAr^+$ and $\psi_{v^+}(r)$ is the wave function of the vibrational level v^+ with energy $E_{v^+} = T_{v^+} - D_0^+$. The potential parameters A, B, C, D, and E were then refined by performing a weighted fit to the experimental vibrational energies T_{v^+} listed in Table 1 and the ground-state rotational constant $B_0 = 0.1409(7)$ cm^{-1} (see eq 7 below) determined by Scurlock et al.[6] As weights, we used the inverse squares of the experimental uncertainties. The potential parameters determined in this way are given in Table 3, the corresponding vibrational energies are compared to the experimental data in Table 1, and the optimized potential is displayed in Figure 1.

To assess the quality of the fit, we computed the weighted root-mean-square (rms) deviation

$$\text{rms} = \sqrt{\frac{\chi^2}{\nu}} \tag{5}$$

where ν is the number of degrees of freedom in the fit and χ^2 is the sum of weighted residuals

$$\chi^2 = \sum_{i=1}^{N} \left(\frac{y_i^{\text{calc}} - y_i^{\text{exp}}}{\sigma_i} \right)^2 \tag{6}$$

The quantities y_i^{calc} and y_i^{exp} denote the calculated and experimental observables, respectively, and σ_i their experimental uncertainties. In the present case, we have $N = 10$ observables (nine vibrational levels for $v^+ = 1{-}9$ and the rotational constant B_0 from ref [6]) and five adjustable parameters (A, B, C, D, and E), and therefore $\nu = 5$. Using eqs 5 and 6, we obtain an rms value of 0.44, i.e., the fit parameters given in Table 3 describe the experimental data well. However, the optimization problem, as described above, does not have a unique solution and the final values of the fit parameters A, B, C, D, and E depend on their initial values. Considering that the fit of the potential parameters to the data of Gardner et al.[21] already yields vibrational term values that typically lie within ~2 cm^{-1} of the experimental ones, we believe that using these parameters as initial values for the optimization procedure is a reasonable choice.

Because the value for A ($= 1.0035 \times 10^{-3}\, E_{\text{h}} \equiv 220.2$ cm^{-1}) is much smaller than D_{e} ($= 1306.5$ cm^{-1}), the Morse potential in eq 2 only makes a small contribution to the binding energy. Moreover, the parameters D ($= 4.0475\, a_0 \approx 2.14$ Å) and E ($= 0.65647\, a_0 \approx 0.35$ Å) indicate that the charge-induced dipole interaction is turned off in the range between ~2 and ~2.3 Å, i.e., at distances shorter than the potential minimum ($R_{\text{e}} = 2.804$ Å). These observations imply that the bond between Mg$^+$ and Ar is dominated by the charge-induced-dipole interaction.

From the potential, the isotopic shifts were calculated by adapting the reduced mass in eq 4. The results are shown in Figure 4, where the solid and dashed lines correspond to the cases where the lowest measured states are $v^+ = 0$ and $v^+ = 1$, respectively. Comparison to the experimentally measured isotopic shifts confirms that the lowest observed vibrational level of the X$^+$ state is indeed $v^+ = 0$.

The Franck–Condon factors of the Mg$^+(3s)\cdot$Ar X$^+$ $^2\Sigma^+$ (v^+) ← Mg$(3s3p)\cdot$Ar a $^3\Pi_0$ $(v'' = 0)$ transitions were calculated by approximating the potential of the Mg$(3s3p)\cdot$Ar a $^3\Pi_0$ state with a Morse potential, the parameters of which were taken from the work of Gaied et al.[12] The calculated Franck–Condon factors are compared with vibrational intensity distributions in Figure 2b. The weak lines appearing on the low-wave-number side of each vibrational line correspond to ^{25}MgAr$^+$ and ^{26}MgAr$^+$.

We computed the rotational constants of all bound levels from the potential specified by eq 2 and Table 3 using the relation

$$hcB_{v^+} = \frac{\hbar^2}{2\mu} \int_0^{\infty} \psi_{v^+}(r) \frac{1}{r^2} \psi_{v^+}(r)\, dr \tag{7}$$

The values obtained for the levels up to $v^+ = 9$ are given in Table 1, and a full list, including the vibrational levels of ^{25}MgAr$^+$ and ^{26}MgAr$^+$, is provided as the Supporting Information.

The molecular constants of MgAr$^+$ in the ground electronic state calculated with our potential are listed in Table 2. Because we only observed vibrational levels with term values up to about half the dissociation energy, our experimental data do not allow for a highly accurate determination of the dissociation energy. Considering possible sources of systematic uncertainties, we estimate $D_0^+ = 1254(60)$ cm^{-1}. From the known ionization energy $(E_I(3s3p\ ^3P_0)/(hc) = 39\,820.65(3)$ cm^{-1}) of the 3s3p $^3P_0$ level of Mg[18] and the adiabatic ionization energy $E_I(a\ ^3\Pi_0)/(hc) = 38\,742.3(20)$ cm^{-1} of the a $^3\Pi_0$ state of MgAr determined in

Table 2. Molecular Constants of the Mg$^+(3s)\cdot$Ar X$^+$ $^2\Sigma^+$ Ground Electronic State[a,b]

$E_I(v^+ = 0)/(hc)$	38 742.3(20)	B_e	0.1429
ω_e	104.49(17)	α_e	0.0042
$\omega_e x_e$	2.36(2)	R_e	2.804
D_0^+	1254(60)	R_0	2.831
D_e	1306.5		

[a]E_I is given with respect to the ground vibrational level of the Mg$(3s3p)\cdot$Ar a $^3\Pi_0$ state. [b]All values are in cm^{-1}, except for R_e and R_0, which are in Å.

Table 3. Parameters Describing the Potential-Energy Function of the X$^+$ $^2\Sigma^+$ State of MgAr$^+$ According to eqs 2 and 3 Obtained in a Least-Squares Fit to the Experimental Vibrational Term Values T_{v^+} and the Ground-State Rotational Constant B_0[a]

A	$1.0035 \times 10^{-3}\, E_{\text{h}}$
B	4.6509
C	6.5170 a_0
D	4.0475 a_0
E	0.65647 a_0
α_{Ar}	11.08 a_0^3

[a]All parameters are given in atomic units.

this work, one can relate the dissociation energies D_0'' and D_0^+ using

$$D_0^+ = D_0'' + E_I(3s3p\ ^3P_0)/(hc) - E_I(a\ ^3\Pi_0)/(hc) \tag{8}$$

From the D_0'' value $(160(40)$ cm$^{-1})$ derived in ref [3], we obtain a value of $1238(40)$ cm^{-1} for D_0^+. Conversely, we can obtain a value for D_0'' from the D_0^+ value corresponding to our potential-energy function $(1254(60)$ cm$^{-1})$. Given that the vibrational wave functions of the $v^+ = 0{-}9$ levels of the Mg$^+(3s)\cdot$Ar X$^+$ $^2\Sigma^+$ state observed in our PFI-ZEKE photoelectron spectrum all have significant amplitudes in the region of internuclear distances beyond 2.5 Å, where the potential is dominated by the charge-induced dipole interaction, we expect our D_0^+ to be accurate to better than 60 cm^{-1}. Our values and previously reported values for D_0^+ and D_0'' are listed in Table 4. Our new value of the dissociation energy of the X$^+$ state agrees with the latest ab initio calculations[2] within experimental uncertainties.

Table 4. Molecular Constants of the X$^+$ $^2\Sigma^+$ State of MgAr$^+$[a]

D_0^+	ω_e	$\omega_e x_e$	R_e	R_0	ref
1254(60)	104.49(17)	2.36(2)	2.804	2.831	this work
1214(165)[b]	99.5(38)	1.5(21)			9
1041					11
1324[b]				2.825(7)	5–7
1180(80)					10
1237(40)					3
1246.7	104.8	2.53	2.822		21
1290(60)	100(3)			2.81(3)	1
1238	104.7	2.68		2.825	2
1235	97.16	3.81	2.91		12

[a]All values are in cm^{-1}, except for R_e and R_0, which are in Å. [b]These values take into account the corrected value of the Mg$^+(3p)\cdot$Ar X$^+$ $^2\Pi_{1/2}$ $(v = 0)$ ← Mg$^+(3s)\cdot$Ar X$^+$ $^2\Sigma^+$ $(v^+ = 0)$ transition reported in ref 26, which is 31 438.5 cm^{-1}.

4.2. Photoionization Dynamics and Intensity Distribution.

The vibrational intensity distribution of the overview PFI-ZEKE photoelectron spectrum and the Franck–Condon factors calculated from our potential of the $Mg^+(3s) \cdot Ar \, X^+ \, ^2\Sigma^+$ state differ strongly (see Figure 2b). The differences are particularly striking for the lowest vibrational levels ($v^+ = 0–2$). With a Franck–Condon factor of $\sim 5 \times 10^{-4}$, the $Mg^+(3s) \cdot Ar \, X^+ \, ^2\Sigma^+ (v^+ = 0) \leftarrow Mg(3s3p) \cdot Ar \, a \, ^3\Pi_0 (v'' = 0)$ band should not have been observed at all. In contrast, the relative intensities of the transitions to high vibrational levels of the $Mg^+(3s) \cdot Ar \, X^+ \, ^2\Sigma^+$ state are in satisfactory agreement with the calculated Franck–Condon factors. The general behavior is reminiscent of similar observations made in studies of the PFI-ZEKE photoelectron spectra of Ag_2[27] and the rare gas dimers[28,29] and can be explained by intensity perturbations resulting from interactions between ionization channels associated with the different rovibrational levels of the $Mg^+(3s) \cdot Ar \, X^+ \, ^2\Sigma^+$ state.

These interactions are depicted schematically in Figure 3c with the examples of the $v^+ = 3$ and 7 thresholds by red arrows connecting the pseudo-continua of very high Rydberg states detected in the PFI-ZEKE photoelectron spectra (illustrated by blue frames for $v^+ = 3$ and 7) and Rydberg states of lower n values belonging to series converging to higher-lying ionization thresholds. The role played by these lower Rydberg states depends on their accessibility from the $Mg(3s3p) \cdot Ar \, a \, ^3\Pi_0 (v'' = 0)$ state, which is governed by the Franck–Condon factors. The same channel interactions are also responsible for the auto-ionization resonances observed in the photoionization spectrum (see Figure 2a), as discussed in general terms in ref 30.

The overall intensity distribution of the PFI-ZEKE photoelectron spectrum can be discussed in terms of the same three regions, labeled (i)–(iii) in Figure 2, of the photoionization spectrum already mentioned in Section 3. The Franck–Condon factors, calculated for the corresponding v^+ channels, are indicated by the thickness of the black arrows in Figure 3c. In region (i), the Franck–Condon factors are extremely small and the intensity observed in the PFI-ZEKE photoelectron spectra is entirely borrowed from transitions to low-lying Rydberg states belonging to series converging on higher vibrational levels. The strength and width of the lines in the PFI-ZEKE spectra are thus very irregular and reflect accidental coincidences with auto-ionization resonances. In region (ii), the Franck–Condon factors are strong enough to lead to a measurable direct-ionization signal and both direct ionization and autoionization contribute to the intensity distribution of the PFI-ZEKE photoelectron spectrum. Because the Franck–Condon factors to the perturbing autoionization resonances are larger than those of associated thresholds detected in the PFI-ZEKE spectrum in this region, the intensity distribution is irregular. In region (iii), beyond $v^+ = 5$, the Franck–Condon factors start decreasing and the relative importance of autoionization compared to direct ionization is rapidly reduced, so that the observed intensities more faithfully reflect the Franck–Condon factors.

The channel interactions are also observed as perturbations of the rotational structure in the high-resolution PFI-ZEKE photoelectron spectra of transitions to low-v^+ levels. These perturbations, marked by asterisks in the spectrum of the $v^+ = 3$ level in Figure 3a, can be recognized experimentally from their response to the successive pulses of the field-ionization sequence. Because they originate from low-n Rydberg states associated with different channels, their positions are independent of the applied electric-field pulses. This aspect is illustrated in Figure 5, which shows the PFI-ZEKE photo-
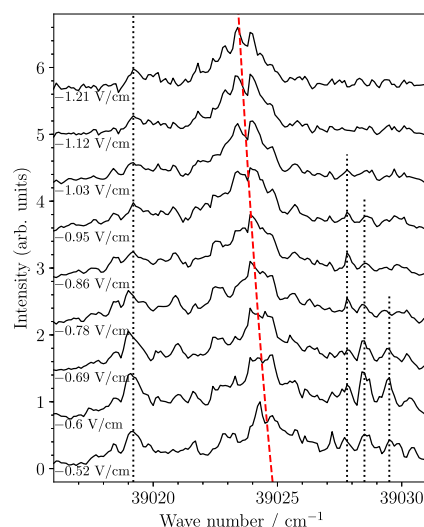

Figure 5. PFI-ZEKE photoelectron spectra of the $Mg^+(3s) \cdot Ar \, X^+ \, ^2\Sigma^+$ $(v^+) \leftarrow Mg(3s3p) \cdot Ar \, ^3\Pi_0 \, (v'' = 0)$ ionizing transition without correction of the field-induced shift of the ionization thresholds. The corresponding electric-field-pulse strengths are indicated below each spectrum. The vertical dotted line indicates the position of a perturber line. The dashed curve indicates the position of the main line of the PFI-ZEKE photoelectron spectrum.

electron spectra obtained for the successive electric-field pulses of the field-ionization sequence. Whereas the position of the central line (at $\sim 39\,024$ cm^{-1}) shifts to lower wave numbers with a shift proportional to $\sqrt{F}$ (F is the electric-field strength), the positions of the satellite lines located at $39\,019.2$ cm^{-1} and between $\sim 39\,028$ and $\sim 39\,031$ cm^{-1} (black dotted lines) are independent of the strength of the pulsed field.

In this way, we could verify that the intensity of the transition to $v^+ = 7$ almost exclusively originates from direct ionization. To simulate its rotational structure, we used the ionization model of Buckingham et al.[20] for the relative intensity of the rotational transitions assuming ionization out of a p orbital and a $^2\Sigma^+$(case b) $\leftarrow \, ^3\Pi_0$(case a) transition. These assumptions lead to contributions to the spectrum of rotational branches with $N^+ - N''$ values $-2, -1, 0, 1,$ and 2 that are labeled as O-, P-, Q-, R-, and S-type branches, respectively, in Figure 3. Further parameters used in the simulation were the rotational constants of the $Mg^+(3s) \cdot Ar \, X^+ \, ^2\Sigma^+$ state given in Table 1, the rotational constants of the two Ω components of the $Mg(3s3p) \cdot Ar \, a \, ^3\Pi_0$ state, $B_0''(^3\Pi_{0^+}) = 0.0835$ cm^{-1} and $B_0''(^3\Pi_{0^-}) = 0.0837$ cm^{-1}, and the $^3\Pi_{0^+}/^3\Pi_{0^-}$ splitting of 0.31 cm^{-1}.[31] The temperature was estimated to be 3 K and the line width (FWHM) was set to 0.6 cm^{-1}. The simulations of the $v^+ = 3$ and 7 bands are shown in Figure 3. As expected, the intensity distribution of the $v^+ = 7$ band is well reproduced by the simulation, whereas the perturbations of the $v^+ = 3$ band discussed above are entirely missing in the simulated spectrum. Unfortunately, we were not able to assign the perturbing levels because of the high spectral density of the photoionization spectrum in this region (see Figure 3a).

5. CONCLUSIONS

This article has presented high-resolution spectroscopic information on the $X^+ \, ^2\Sigma^+$ ground state of $MgAr^+$ by PFI-ZEKE photoelectron spectroscopy and MATI spectroscopy. The observation of vibrational levels as high as $v^+ = 9$ and the demonstrated ability to produce $MgAr^+$ in selected vibrational

levels of the X$^+$ state opens up the prospects of carrying out state-selected photodissociation and photoionization experiments on MgAr$^+$, accessing a broader range of electronic states MgAr$^+$ than previously possible and even characterizing the doubly charged MgAr^{2+} ion. Work in these directions is currently underway in our laboratory.

■ ASSOCIATED CONTENT

Ⓢ Supporting Information

The Supporting Information is available free of charge at https://pubs.acs.org/doi/10.1021/acs.jpca.9b10435.

Calculated vibrational levels and rotational constants of the X$^+$ $^2\Sigma^+$ ground state of ^{24}MgAr$^+$, ^{25}MgAr$^+$, and ^{26}MgAr$^+$ (PDF)

■ AUTHOR INFORMATION

Corresponding Author
*E-mail: frederic.merkt@phys.chem.ethz.ch.

ORCID Ⓞ

Dominik Wehrli: 0000-0002-6885-8674

Notes
The authors declare no competing financial interest.

■ ACKNOWLEDGMENTS

■ REFERENCES

(1) Bellert, D.; Breckenridge, W. H. Bonding in ground-state and excited-state A$^+$Rg van der Waals ions (A = atom, Rg = rare-gas atom): a model-potential analysis. *Chem. Rev.* **2002**, *102*, 1595−1622.

(2) Tuttle, W. D.; Harris, J. P.; Zheng, Y.; Breckenridge, W. H.; Wright, T. G. Hybridization and covalency in the group 2 and group 12 metal cation/rare gas complexes. *J. Phys. Chem. A* **2018**, *122*, 7679−7703.

(3) Massick, S.; Breckenridge, W. H. A determination of the ionization threshold for the Mg(3s3p ^{3}P$_0$)·Ar($^3\Pi_0^-$) metastable state: the bond energy of MgAr$^+$. *Chem. Phys. Lett.* **1996**, *257*, 465−470.

(4) Pilgrim, J. S.; Yeh, C. S.; Duncan, M. A. Photodissociation spectroscopy of Mg$^+$−Ar. *Chem. Phys. Lett.* **1993**, *210*, 322−326.

(5) Pilgrim, J. S.; Yeh, C. S.; Berry, K. R.; Duncan, M. A. Photodissociation spectroscopy of Mg$^+$−rare gas complexes. *J. Chem. Phys.* **1994**, *100*, 7945.

(6) Scurlock, C. T.; Pilgrim, J. S.; Duncan, M. A. Rotationally resolved photodissociation spectroscopy of Mg$^+$−Ar. *J. Chem. Phys.* **1995**, *103*, 3293.

(7) Scurlock, C. T.; Pilgrim, J. S.; Duncan, M. A. Erratum: Rotationally resolved photodissociation spectroscopy of Mg$^+$−Ar [J. Chem. Phys. 103, 3293 (1995)]. *J. Chem. Phys.* **1996**, *105*, 7876.

(8) Bennett, R. R.; McCaffrey, J. G.; Wallace, I.; Funk, D. J.; Kowalski, A.; Breckenridge, W. H. A laser spectroscopic study of the X $^1\Sigma_0^+$ − C $^1\Pi_1$ transition of MgAr: evidence for Łambda-type doubling. *J. Chem. Phys.* **1989**, *90*, 2139.

(9) Le Roy, R. J. Near-dissociation expansions and dissociation energies for Mg$^+$−(rare gas) bimers. *J. Chem. Phys.* **1994**, *101*, 10217.

(10) Hoshino, H.; Yamakita, Y.; Okutsu, K.; Suzuki, Y.; Saito, M.; Koyasu, K.; Ohshimo, K.; Misaizu, F. Photofragment imaging from mass-selected ions using a reflectron mass spectrometer I. Development of an apparatus and application to Mg$^+$−Ar complex. *Chem. Phys. Lett.* **2015**, *630*, 111−115.

(11) Bauschlicher, C. W., Jr.; Partridge, H. A study of the X $^2\Sigma^+$ and A $^2\Pi$ states of MgAr$^+$ and MgKr$^+$. *Chem. Phys. Lett.* **1995**, *239*, 241−245.

(12) Gaied, W.; Habli, H.; Oujia, B.; Gadea, F. X. Theoretical study of the MgAr molecule and its ion Mg$^+$Ar: potential energy curves and spectroscopic constants. *Eur. Phys. J. D* **2011**, *62*, 371−378.

(13) Génévriez, M.; Wehrli, D.; Agner, J. A.; Merkt, F. PFI-ZEKE photoelectron spectroscopy of positively charged ions: illustration with Mg$^+$. *Int. J. Mass Spectrom.* **2019**, *435*, 209−216.

(14) Designed by Leutwyler, S.; Frey, H. M. *Constructed by the Mechanical and Electronics Workshops of the Department of Chemistry and Biochemistry, Freiestrasse 3*; Universität Bern: CH-3012 Bern, 2014.

(15) Bennett, R. R.; McCaffrey, J. G.; Breckenridge, W. H. A spectroscopic characterization of the ã $^3\Pi_0^-$, A $^3\Pi_0^+$, and E $^3\Sigma^+$ states of the MgAr van der Waals molecule. *J. Chem. Phys.* **1990**, *92*, 2740.

(16) Müller-Dethlefs, K.; Schlag, E. W. High-resolution zero kinetic energy (ZEKE) photoelectron spectroscopy of molecular systems. *Annu. Rev. Phys. Chem.* **1991**, *42*, 109−136.

(17) Hollenstein, U.; Seiler, R.; Schmutz, H.; Andrist, M.; Merkt, F. Selective field ionization of high Rydberg states: application to zero-kinetic-energy photoelectron spectroscopy. *J. Chem. Phys.* **2001**, *115*, 5461−5469.

(18) Kramida, A.; Ralchenko, Y.; Reader, J.; NIST ASD Team. *NIST Atomic Spectra Database* (ver. 5.6.1), [Online]. National Inåstitute of Standards and Technology: Gaithersburg, MD. Available: https://physics.nist.gov/asd [2019, January 29], 2018.

(19) Zhu, L.; Johnson, P. Mass analyzed threshold ionization spectroscopy. *J. Chem. Phys.* **1991**, *94*, 5769−5771.

(20) Buckingham, A. D.; Orr, B. J.; Sichel, J. M. Angular distribution and intensity in molecular photoelectron spectroscopy I. General theory for diatomic molecules. *Philos. Trans. R. Soc. London, Ser. A* **1970**, *268*, 147−157.

(21) Gardner, A. M.; Withers, C. D.; Graneek, J. B.; Wright, T. G.; Viehland, L. A.; Breckenridge, W. H. Theoretical study of M$^+$−RG and M^{2+}−RG complexes and transport of M$^+$ through RG (M = Be and Mg, RG = He-Rn). *J. Phys. Chem. A* **2010**, *114*, 7631−7641.

(22) Gaiser, C.; Fellmuth, B. Polarizability of helium, neon, and argon: new perspectives for gas metrology. *Phys. Rev. Lett.* **2018**, *120*, No. 123203.

(23) Manolopoulos, D.; Wyatt, R. Quantum scattering via the log derivative version of the Kohn variational principle. *Chem. Phys. Lett.* **1988**, *152*, 23−32.

(24) Rescigno, T. N.; McCurdy, C. W. Numerical grid methods for quantum-mechanical scattering problems. *Phys. Rev. A* **2000**, *62*, No. 032706.

(25) Telnov, D. A.; Chu, S. Multiphoton detachment of H$^-$ near the one-photon threshold: Exterior complex-scaling-generalized pseudospectral method for complex quasienergy resonances. *Phys. Rev. A* **1999**, *59*, 2864.

(26) Génévriez, M.; Wehrli, D.; Merkt, F. *Mol. Phys.* DOI: 10.1080/00268976.2019.1703051.

(27) Yeretzian, C.; Hermann, R. H.; Ungar, H.; Selzle, H. L.; Schlag, E. W.; Lin, S. H. Breakdown of the Born-Oppenheimer approximation in ZEKE states of Ag$_2$. *Chem. Phys. Lett.* **1995**, *239*, 61−66.

(28) Signorell, R.; Merkt, F. The first electronic states of Ar$_2^+$ studied by high resolution photoelectron spectroscopy. *J. Chem. Phys.* **1998**, *109*, 9762−9771.

(29) Signorell, R.; Hollenstein, U.; Merkt, F. High-resolution photoelectron spectroscopic study of the first electronic state of Kr$_2^+$. *J. Chem. Phys.* **2001**, *114*, 9840−9851.

(30) Merkt, F.; Softley, T. P. Rotational line intensities in zero kinetic energy photoelectron spectroscopy (ZEKE-PES). *Int. Rev. Phys. Chem.* **1993**, *12*, 205−239.

(31) Massick, S.; Breckenridge, W. H. Spectroscopic characterization of the $^3\Delta(4d)$, $^3\Pi(4d)$, $^3\Sigma^+(4d)$, and $^3\Pi(5p)$ Rydberg states of the MgAr van der Waals molecule. *J. Chem. Phys.* **1997**, *106*, 2171.